

Soft, Skin-Interfaced Microfluidic Systems with Passive Galvanic Stopwatches for Precise Chronometric Sampling of Sweat

Amay J. Bandodkar, Jungil Choi, Stephen P. Lee, William J. Jeang, Prophecy Agyare, Philipp Gutruf, Siqing Wang, Rebecca A. Sponenburger, Jonathan T. Reeder, Stephanie Schon, Tyler R. Ray, Shulin Chen, Sunita Mehta, Savanna Ruiz, and John A. Rogers*

Comprehensive analysis of sweat chemistry provides noninvasive health monitoring capabilities that complement established biophysical measurements such as heart rate, blood oxygenation, and body temperature. Recent developments in skin-integrated soft microfluidic systems address many challenges associated with standard technologies in sweat collection and analysis. However, recording of time-dependent variations in sweat composition requires bulky electronic systems and power sources, thereby constraining form factor, cost, and modes of use. Here, presented are unconventional design concepts, materials, and device operation principles that address this challenge. Flexible galvanic cells embedded within skin-interfaced microfluidics with passive valves serve as sweat-activated “stopwatches” that record temporal information associated with collection of discrete microliter volumes of sweat. The result allows for precise measurements of dynamic sweat composition fluctuations using in situ or ex situ analytical techniques. Integrated electronics based on near-field communication (NFC) protocols or docking stations equipped with standard electronic measurement tools provide means for extracting digital timing results from the stopwatches. Human subject studies of time-stamped sweat samples by in situ colorimetric methods and ex situ techniques based on inductively coupled plasma mass spectroscopy (ICP-MS) and chlorodimetry illustrate the ability to quantitatively capture time-dynamic sweat chemistry in scenarios compatible with field use.

Human eccrine sweat contains a rich composition of nearly 60 known physiologically relevant biochemicals including metabolites, electrolytes, vitamins, amino acids, exogenous drugs, and small proteins.^[1] Existing skin-interfaced sweat sensors can, however, only detect a handful of these biochemicals.^[2–4] Sophisticated laboratory-based analytical instruments allow for ex situ detection of a broad scope of analytes beyond this limited set, with extreme precision and accuracy.^[5,6] Unfortunately, approaches in sample collection that use absorbent pads or microtubes mix sweat obtained throughout the course of a collection period, limiting measurements to only time-averaged compositions. Such methods severely restrict opportunities for comprehensive understanding of critical time-dependent variations in sweat composition and their relation to human physiology. Recent developments in the field of soft microfluidics^[7] and passive capillary burst valves (CBVs)^[8,9] enable sequential collection of pristine

Dr. A. J. Bandodkar, W. J. Jeang, Dr. J. T. Reeder, Dr. S. Mehta, S. Ruiz,
Prof. J. A. Rogers
Department of Materials Science and Engineering
Northwestern University
Evanston, IL 60208, USA
E-mail: jrogers@northwestern.edu

Dr. A. J. Bandodkar, S. P. Lee, W. J. Jeang, Dr. J. T. Reeder, Dr. S. Mehta,
S. Ruiz, Prof. J. A. Rogers
Center for Bio-Integrated Electronics
Simpson Querrey Institute for BioNanotechnology
Northwestern University
Evanston, IL 60208, USA

Prof. J. Choi
School of Mechanical Engineering
Kookmin University
Seoul 02707, Republic of Korea

 The ORCID identification number(s) for the author(s) of this article can be found under <https://doi.org/10.1002/adma.201902109>.

S. P. Lee
Epicore Biosystems Inc.
Cambridge, MA 02139, USA

P. Agyare
Department of Neuroscience
Northwestern University
Evanston, IL 60201, USA

Prof. P. Gutruf
Department of Biomedical Engineering
University of Arizona
Tucson, AZ 85721, USA

S. Wang
School of Materials Science and Engineering
Tsinghua University
Beijing 100084, China

R. A. Sponenburger
Quantitative Bio-Element Imaging Center
Northwestern University
Evanston, IL 60208, USA

DOI: 10.1002/adma.201902109

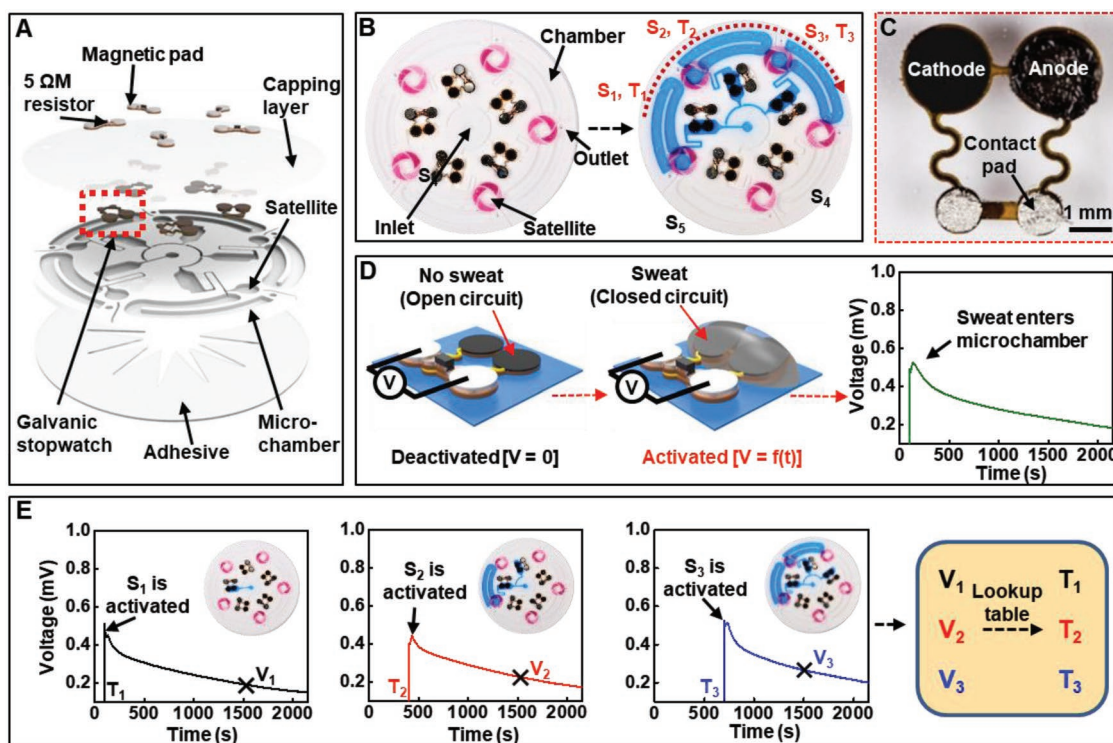


Figure 1. A) Schematic exploded view illustration of a chronosampling soft microfluidic sweat device with embedded galvanic stopwatches. B) Photographs of the device before and during filling with a blue dye in water. The dotted arrow displays the direction of filling of microchambers. C) Image of a galvanic stopwatch. D) Diagram illustrating the operation of the stopwatch and a typical voltage–time curve. E) Representative voltage–time plots demonstrating activation of different stopwatches at different time points corresponding to filling of respective microchambers. A calibrated lookup table defines the initial filling time of each microchamber based on a measurement of instantaneous stopwatch voltages at any time, as marked on the characteristic voltage decay plots. S_i , stopwatch number; V_i , instantaneous stopwatch voltage; T_i , time at which a stopwatch is activated.

microliter volumes of sweat in a series of chambers, with negligible sample intermixing. The inability to determine the time at which each chamber fills prevents the determination of temporal variations in composition. Standard electronic clocks inserted into the microfluidic system could, in principle, record this time information, but this type of approach adds cost, bulk, size, and weight to the overall platform, particularly for those that require batteries for power supply. The resulting characteristics reduce the appeal of this design approach for demanding use-case scenarios encountered in sports, military, rehabilitation, and related applications.

Here, we introduce a unique solution that leverages simple, inexpensive, spontaneous galvanic cells for in situ time recording of the sweat collection process. We refer to these

time-stamping cells as “galvanic stopwatches.” The present work demonstrates these stopwatches in soft microfluidic systems with five chambers interconnected with passive valves that enable chronometric collection of sweat samples with negligible intermixing (Figure 1A). These single-use, low cost sweat collection systems avoid inadvertent sample contamination caused by previous cycles of use. Galvanic cells offer a battery-free approach to tracking the dynamics of the filling of sweat into the device. Each chamber captures $\approx 50 \mu\text{L}$ of sweat, as a sufficient sample size for detection of a wide range of analytes using multiple instruments. Additionally, every chamber includes an associated satellite assay zone for in situ colorimetric detection of a desired analyte. Skin anatomy and collection area dictate the total amount of sweat captured from an individual for a given period of perspiration. The concepts can easily be extended to larger, or smaller, numbers of chambers, to address requirements in time resolution and sample volumes. The soft construction of the microfluidic patch supports robust, water-tight, irritation-free interfaces to the skin. Carefully designed CBVs direct sweat flow, resulting in sequential filling of the chambers with negligible intermixing (Figure 1B). The operation of the galvanic stopwatch at the entrance of each chamber provides a mechanism to determine the collection time of each sample aliquot.

Each stopwatch consists of a solid-state anode and cathode with a fixed load connected across it (Figure 1C). A redox agent

S. Schon
Department of Mechanical and Process Engineering
ETH Zurich
CH-8092 Zurich, Switzerland

Prof. T. R. Ray
Department of Mechanical Engineering
University of Hawai'i at Mānoa
Honolulu, HI 96822, USA

S. Chen
Department of Biomedical Engineering
Northwestern University
Evanston, IL 60208, USA

(tertrathiafulvalene) functionalizes the anode while an oxygen reducing electrode (platinized carbon) acts as the cathode (Figure S1A, Supporting Information). Figure 1D illustrates the working principle. In the absence of sweat these stopwatches behave as open circuits. Exposure to sweat connects the two electrodes, completing the electrical circuit to generate a voltage that decays in a well-characterized time-dependent fashion. As the microchambers fill sequentially, incoming sweat activates the corresponding stopwatches at different times. The voltage readings provide a means for determining the time of collection for each chamber (Figure 1E). These voltages can be obtained with a battery-free NFC module for use in the field or a portable data acquisition docking station for application in controlled settings. These schemes for collection, extraction, and time tracking provide versatile options for analysis of sweat dynamics in a manner that is compatible with any in situ or ex situ analysis technique (i.e., spectroscopy, calorimetry, or electrochemistry).

The primary design exploits a reusable NFC data acquisition module (Figure 2A) that wirelessly transmits voltage values to a smartphone or other NFC-enabled reader. Design and fabrication details appear in the Experimental Section (Supporting Information). This lightweight (≈ 2 g), compact (diameter: 40 mm) platform consists of a thin, laser-patterned flexible copper–polyimide–copper printed circuit board (fPCB) populated with commercially available electronic components, each of which is less than 1 mm in height. As shown in the simplified schematic illustration in Figure 2A, the system contains a low-power microcontroller with an integrated analog to digital converter, NFC electrically erasable programmable memory (NFC EEPROM) with a power harvester, and an analog signal conditioning circuit that differentially measures voltage across each of the galvanic stopwatches. The signal conditioner takes advantage of the high common-mode rejection of the instrumentation amplifier to accurately measure each electrochemical cell and it rejects common-mode potentials that span across the sweat channel that connects each of the cells. A low cross-talk 8:1 analog switch multiplexes each of the electrochemical cells to the amplifier to provide the ability to measure several channels while reducing component count. Neodymium magnets (diameter: 1 mm; thickness: 1 mm) bonded to contacts on the fPCB enable robust, reversible electromechanical attachment to ferromagnetic pads connected to the contact pads of the galvanic stopwatches embedded within the underlying microfluidic system.^[10] Figure S1B in the Supporting Information shows a transverse section schematic illustration of a stopwatch embedded in the microfluidic system and interfaced to a resistive load via a pair of ferromagnetic contact pads and a flexible copper support.

An alternative approach relies on a docking station that utilizes conventional, battery-powered data acquisition electronics and additional sweat sample extraction capabilities (Experimental Section, Figure S2A, Supporting Information). Specifically, this docking station interfaces to a 16 bit, 8-channel data acquisition system capable of sampling at a maximum aggregate rate of 400 ksps (National Instruments USB-6212) and connects to a display unit (i.e., a laptop computer). Magnetic contacts, similar to those described for the NFC system, serve as reversible electromechanical attachments

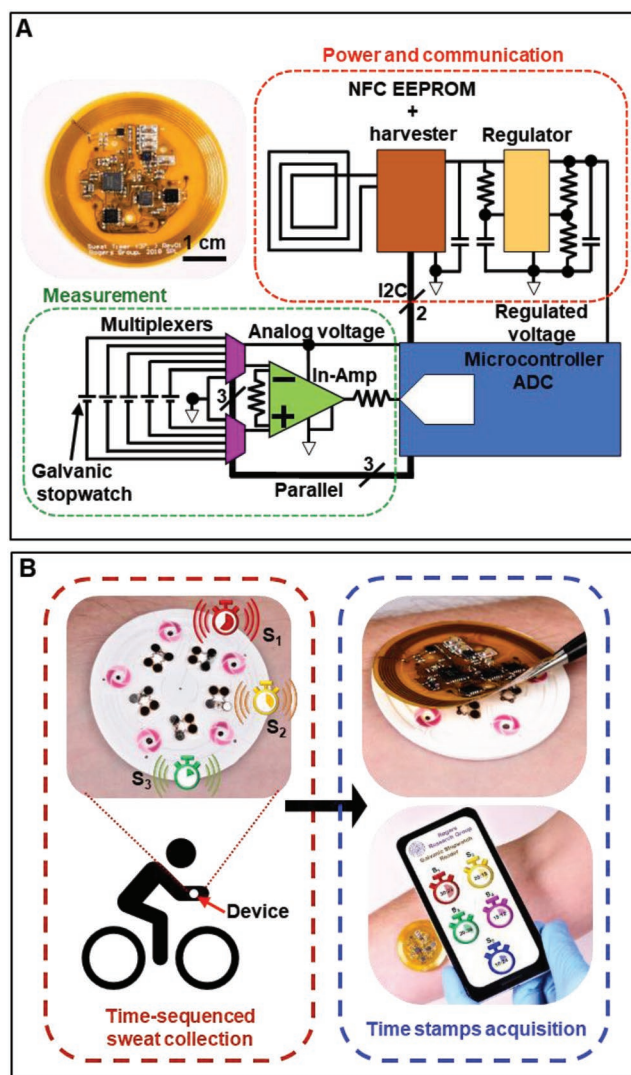


Figure 2. A) Photograph and schematic illustration of a flexible, battery-free NFC electronic system for capturing and wirelessly transmitting voltages on each stopwatch. B) Flowchart delineating standard device usage consisting of on-body sequential sample collection during physical activity (red box) and logging of time stamps using the NFC electronics module (blue box). The smartphone image illustrates a simulated graphical user interface, with a suggestive design.

to corresponding magnetic contact pads of the stopwatches. Additional features include a slidable housing for a mechanical punch and micropipette tip slots located around the periphery. The high input impedance (10 G Ω), low input bias current (100 pA), low cross-talk (-75 dB), and high common-mode rejection (100 dB) allow accurate recordings of voltage signals generated by the stopwatches.

The combined system measures the electrochemical cells, logs data, and converts the cell voltages to time points based on a lookup table preloaded in the software. This table draws upon the average of voltage decay curves of five different stopwatches produced in a single batch. Such curves correspond to continuous measurements of the voltage values of each stopwatch upon exposure to phosphate buffer solution using a

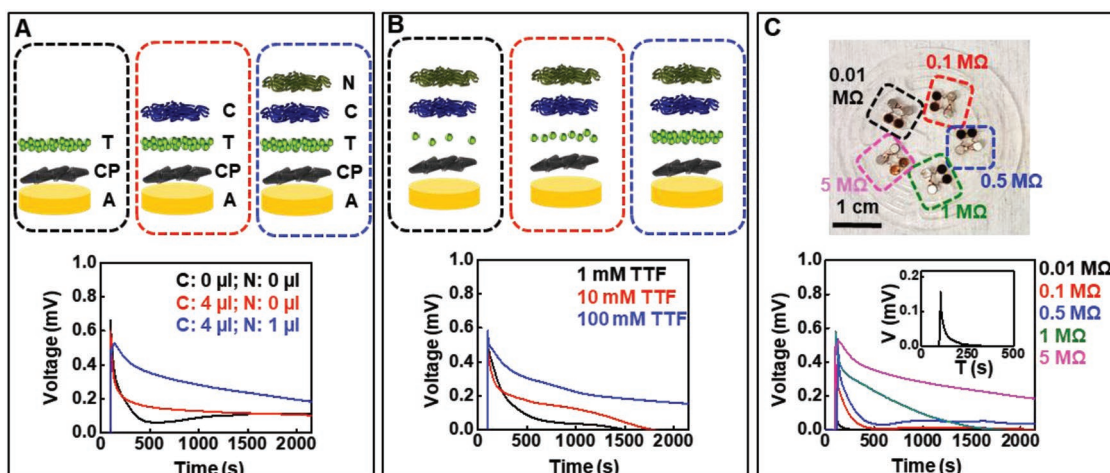


Figure 3. A) Effect of polymeric barriers on stopwatch sensitivity (A: gold; CP: carbon nanotube paper; T: tetrathiafulvalene; C: Chitosan; N: Nafion). B,C) Effect of tetrathiafulvalene concentration (B), and external load (C) on stopwatch sensitivity.

data acquisition hardware (AI Instruments, CO, USA). The docking station operates using a custom graphical user interface (GUI, Figure S2B, Supporting Information) which runs on LabVIEW 2017 and builds around a finite measurement template that uses a state machine with event-driven user interface design pattern. As each event occurs, such as making a measurement or logging the results, the application runs the respective instruction sequence. The application also supports user-definable input voltage range, sampling rate, the number of values per averages, and a location to save a log file. For experiments described here, the voltage range is +1 to −1 V, the sampling rate is 10 ksp/s and each measured value corresponds to an average of 32 readings. The program converts measured voltage values to corresponding time values based on a calibrated look-up table.

A typical use-case scenario involves application of the microfluidic device to the skin followed by engagement in a physical activity (Figure 2B). Sweat that emerges from the surface of the skin sequentially fills collection chambers separated by CBVs and concurrently activates the corresponding stopwatches. Mounting the NFC module onto the device allows for acquisition, processing, and display of the data via an NFC interface to a smartphone. Additionally, the camera of the smartphone supports capture of images of colorimetric assays within the microfluidic structure for in situ biochemical analysis. Alternatively, the docking station can be used for logging data and extracting sweat samples. The process for extracting sweat samples involves removing the device from the skin and then excising the inlet and the microchannel that connects the reservoirs with a mechanical punch (Figure S2C, Supporting Information). This procedure isolates each chamber during sample extraction using a micropipette (Figure S2D, Supporting Information). Figure S2E in the Supporting Information provides a magnified view of the steps. Sweat samples captured in this manner can be transferred in microtubes for further study in an analytical laboratory.

The operation of the stopwatches draws inspiration from solid-state fuel cells.^[11] The devices include an anode and a cathode in a thin, flexible (thickness: $\approx 75 \mu\text{m}$), ultralight

(<1 mg), miniaturized (5 mm \times 2 mm) form factor. Design of the galvanic stopwatches involve careful selection of materials for the anode and the cathode. The active material for the anode is tetrathiafulvalene (TTF) which has a low oxidation potential ($\approx 0 \text{ V vs Ag/AgCl}$).^[12] Platinized carbon forms the catalytic layer for facile reduction of oxygen ($\approx 0.6 \text{ V vs Ag/AgCl}$).^[12] A combination of these half-cell reactions results in a dry, solid-state galvanic cell that spontaneously produces a maximum electromotive force around 0.6 V when contacted with an electrolyte solution such as sweat. The composition/thickness of the polymeric diffusion barriers (Figure 3A), the amount of TTF (Figure 3B), and the resistance of the external load (Figure 3C) determine the voltage–time response.

Stopwatches with no polymeric barriers suffer from poor reproducibility (maximum RSD $\approx 40\%$, $n = 3$). The reproducibility of stopwatches produced in a single batch improves (maximum RSD < 15%; $n = 5$; Figure S3A, Supporting Information) with increasing numbers of Nafion and chitosan overlayers. Here, RSD calculation relies on error in measured voltage at a given time. The polymeric coatings serve two purposes—their barrier properties minimize leaching of TTF into the sample, and their insulating nature increases the internal resistance of the galvanic cell resulting in slow, well-defined voltage decay. The positively charged chitosan polymers electrostatically bond to the negatively charged Nafion chains to ensure high quality coatings. The data represented in Figure 3 demonstrate that a careful combination of active anodic and cathodic materials, with polymeric coatings as barriers and insulating layers yield stopwatches with desired sensitivity and operational lifespan. Unavoidable variations associated with manual fabrication steps, compositional differences in the carbon nanotube paper (CNT) paper, and dispersion of the platinized carbon ink likely contribute to uncertainties in voltage response. The most significant errors arise at early times after stopwatch activation. Here, variations in the rate of sweat filling the gap between the anode and cathode could lead to slight discrepancies. All experiments reported here use the same electrode composition (Experimental Section; Supporting Information) and an external load of 5 M Ω to produce stopwatches with good

sensitivity and reproducibility as shown in Figure S3A in the Supporting Information.

Tests of the microfluidic systems on human subjects reveal average sweat flow rates in the range $\approx 3\text{--}5\ \mu\text{L min}^{-1}$ for designs used here. Benchtop experiments establish that the stopwatches perform similarly across a range of flow rates between 1 and $10\ \mu\text{L min}^{-1}$ (Figure S3B, Supporting Information). For flow rates of less than $1\ \mu\text{L min}^{-1}$, the responses exhibit enhanced effects related to the slow, gradual filling of the chamber. In general, judicious selection of stopwatch size, microfluidic chamber volume, electrode compositions, and external loads offers robust operation across nearly any desired range of flow rates. As illustrated in Figure S3C in the Supporting Information, the thin, flexible nature of the stopwatches and the use of serpentine interconnects leads to performance that is largely independent of bending stresses commonly encountered in practical applications. Studies of effects of temperature indicate stable responses across a physiologically relevant range (Figure S3D, Supporting Information).^[13]

Human sweat contains various biochemicals.^[1] Furthermore, the ionic conductivity of the sweat changes with physiological state and can vary significantly across populations.^[14] Since the stopwatches rely on sweat as an electrolyte, these factors could be important. Figure S3E,F in the Supporting Information indicates minimal effects of such sweat composition variations. In the operation of a stopwatch, the sweat only serves the role of an electroinactive electrolyte to complete the electrical circuit. The composition of the stopwatch electrodes, rather than the sweat chemistry, dictates the voltage decay profiles. Hence, person-to-person variations in sweat composition have negligible effect on the operation. Figure S3G in the Supporting Information shows that the performance is similar under under quiescent and vigorous movement conditions.

Figure S3H in the Supporting Information illustrates the responses of stopwatches from three different batches. The data exhibit a maximum RSD of $\approx 25\%$ in estimating time stamps. In present work, a unique lookup table is generated for each batch using five different stopwatches to achieve timekeeping with high accuracy. Table S1 in the Supporting Information compares the actual time elapsed after stopwatch activation during a benchtop experiment and time estimated from a lookup table. The data reveal that the estimated time varies by a couple of minutes compared to the actual time. The most significant errors arise at times shortly after stopwatch activation. Here, variations in the rate of sweat filling the gap between the anode and cathode lead to uncertainties. These

deviations are acceptable for most practical applications, where the filling of each microchamber at natural rates of sweating ($12\text{--}120\ \mu\text{L h}^{-1}\ \text{cm}^{-2}$)^[7] typically requires several minutes. Automation of the stopwatch fabrication process will further improve the reproducibility and may obviate the need for separate lookup tables.

The soft microfluidic systems exploit concepts and designs reported previously.^[15] Here, molded silicone (elastic modulus: $\approx 1\ \text{MPa}$) membranes include an inlet hole, a series of five collection chambers each with an associated stopwatch, a satellite zone for in situ colorimetric chemical analysis and an outlet for sweat extraction via a micropipette. The device bonds to the skin via a laser-patterned adhesive layer. Each chamber holds $\approx 50\ \mu\text{L}$ of sweat, thus providing sufficient volumes for most analytical tools. Microchannels that connect the chambers include passive CBVs that enable sequential collection of incoming sweat and maintain physical separation of the sweat aliquots collected in each chamber. Careful design of the critical dimensions including those of the CBVs, chambers, interconnecting microchannels, inlets, and outlets facilitates entry of sweat into the device at pressures generated by the eccrine glands, with negligible back pressure that might otherwise hinder flow (Figure S4A, Supporting Information).^[7] These polydimethylsiloxane (PDMS)-based microfluidic devices are designed for a single workout session. PDMS offers favorable mechanical properties, biocompatibility, ease of processability, and widespread use within academia and industry. This elastomer also allows storage of sweat samples without significant sample evaporation for applications explored in the present work. Collection and storage of sweat samples over longer periods can be realized with low water permeability elastomers such as styrenic block copolymers^[16] and polyisobutylene.^[17] Judicious choices for channel geometries, wall thicknesses, outlet dimensions, and other features of the microfluidics can further limit evaporation and associated errors in concentration analysis.

Tests using aqueous solutions of colored food dyes reveal negligible intermixing after 1 h of sample introduction (Figure 4A; Figure S4B, Supporting Information). Color analysis relies on the region marked in Figure S4B in the Supporting Information. As mentioned in the manuscript, extraction of individual sweat samples involves excision of the inlet and the interconnecting microchannel (Figure S2E, Supporting Information). The region of image analysis lies adjacent to the excision boundary. Thus, colorimetric analysis of this region simulates evaluation of chemical contamination between samples (Figure S4B,

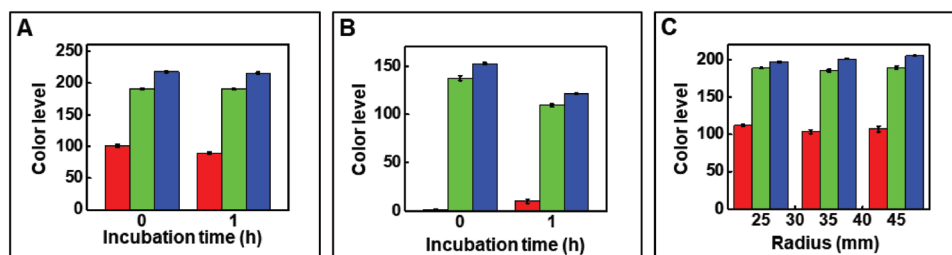


Figure 4. A–C) Comparison of RGB values extracted from images of the device at the interface of the stopwatch chamber and corresponding collection chamber at an incubation time $t = 0$ and 1 h under quiescent conditions (A), after mechanical vibration (B), and after bending to different radii of curvature (C).

Supporting Information). Similar experiments performed on the device when subjected to inertial forces (Figure 4B) and mechanical deformations (Figure 4C) further support the ability to capture discrete sweat samples during vigorous exercise when applied to body parts having different curvatures, with minimal contamination between adjacent chambers. Studies of effects of mechanical deformation involved wrapping the device over curved surfaces of varying radii ($R = 25, 35, \text{ and } 45 \text{ mm}$). Tests of inertial forces involved placing the device on an orbital shaker ($\approx 150 \text{ rpm}$) for 1 h.

The human body excretes electrolytes and minerals during perspiration and physical exertion. Replenishment of these biochemicals is essential for recovery and efficient functioning of the human body.^[18–20] The human trials reported here quantify sweat chemistry, including the concentrations of sodium, potassium, chloride, magnesium, calcium, hydronium ions, copper, and iron during workouts. The total amount of sweat generated, and hence collected by the device, is directly proportional to exercise intensity.^[21] The trials require the subjects to cycle at different intensities (fixed intensity for a given bout) to yield varying sweat rates and different extents of device filling. Such tests allow studies of the effects of exercise intensity on sweat chemistry. Tests involve healthy subjects (three males, one female) with the device mounted on the outer forearm while cycling on a stationary bike at varying intensities and times to generate sweat rates and extents of filling over a practically relevant range. The protocol was approved by the Institutional Review Board of Northwestern University (IRB: STU00208494). Written informed consent was obtained for all subjects. Shaving of the target skin region and thoroughly cleaning the area with alcohol wipes prior to device application improves adhesion and minimizes contamination due to residual chemicals, oils, and dirt on the skin. After exercise, measurement using either of the two previously described data acquisition systems yields voltage values and, by use of calibrated look-up tables, time stamps from the stopwatches.

The first set of trials focuses on in situ measurement of sweat chloride and pH. Here, the devices include colorimetric assays embedded in each satellite zone of the chambers with color reference markers to facilitate determination of color information (Figure S5A,B, Supporting Information) using an image analysis protocol described in previous work.^[9,10,22] The narrow micro-channel that isolates each satellite from the corresponding stopwatch and collection chamber limits diffusion of colorimetric assay reagents and minimizes sample contamination and interference with the electrochemical reactions in the stopwatch (Figure S5C–E, Supporting Information).

Recent studies on otherwise similar colorimetric platforms provide extensive details on the effects of storage, ambient light, and chemical interference on sensor performance, including operational stability.^[9,10] The results highlighted in Figure S5C,D in the Supporting Information emulate practical situations where a sample solution of known chloride concentration ($40 \times 10^{-3} \text{ M}$) is continuously passed into the device at physiologically relevant flow rates ($3 \mu\text{L min}^{-1}$) for 1 h. The color signal generated by the chloride assay remains consistent ($<5\%$ change) throughout. The sweat composition measurements appear in Figure 5 and Figure S6 (Supporting Information). The sweat chloride concentration increases with time and then gradually decreases. Moreover, the absolute concentrations exhibit a dependence on sweat rate, with higher concentrations recorded for higher sweat rates, consistent with previous reports.^[23] Gradual decreases in chloride concentration occur toward the end of cycling bouts due, at least in part, to decreases in the sweat rate as the subjects experience fatigue. The sweat pH, on the other hand, shows little dependence on sweat rate or time, with a slight increase during the final stages of high-intensity exercise as observed in previous studies.^[24]

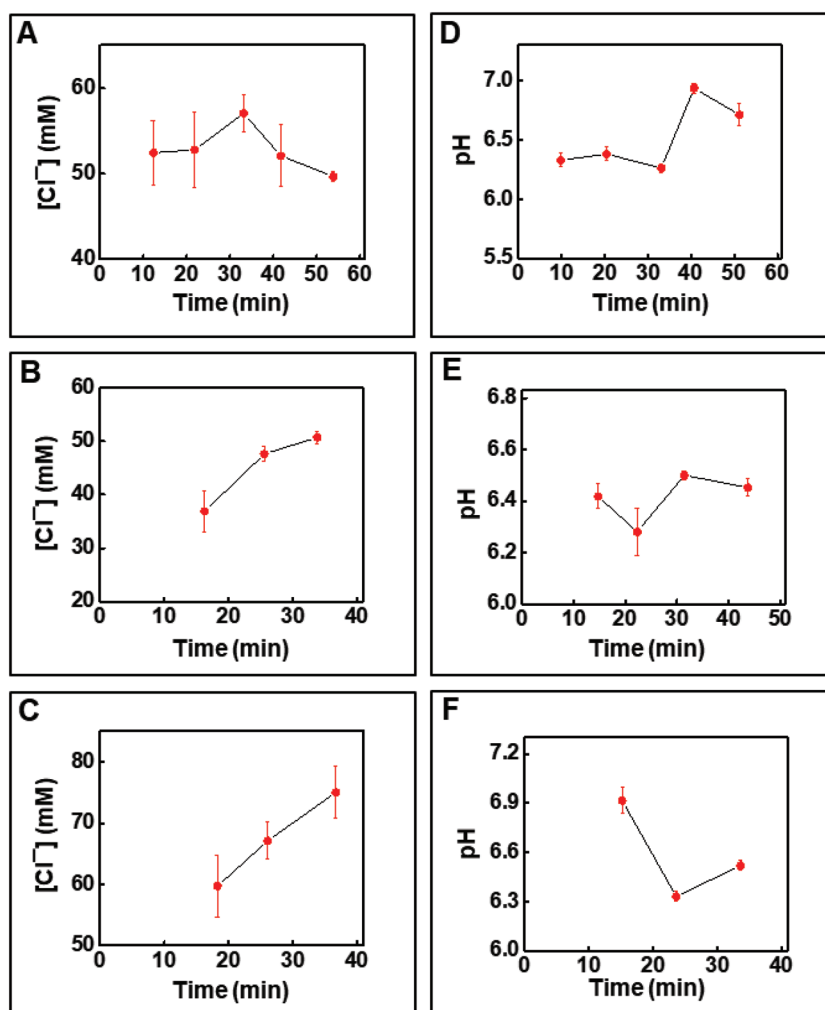


Figure 5. Temporal variations in sweat: A–C) chloride concentrations and D–E) pH levels with varying cycling intensities, as determined using in situ colorimetric sensors.

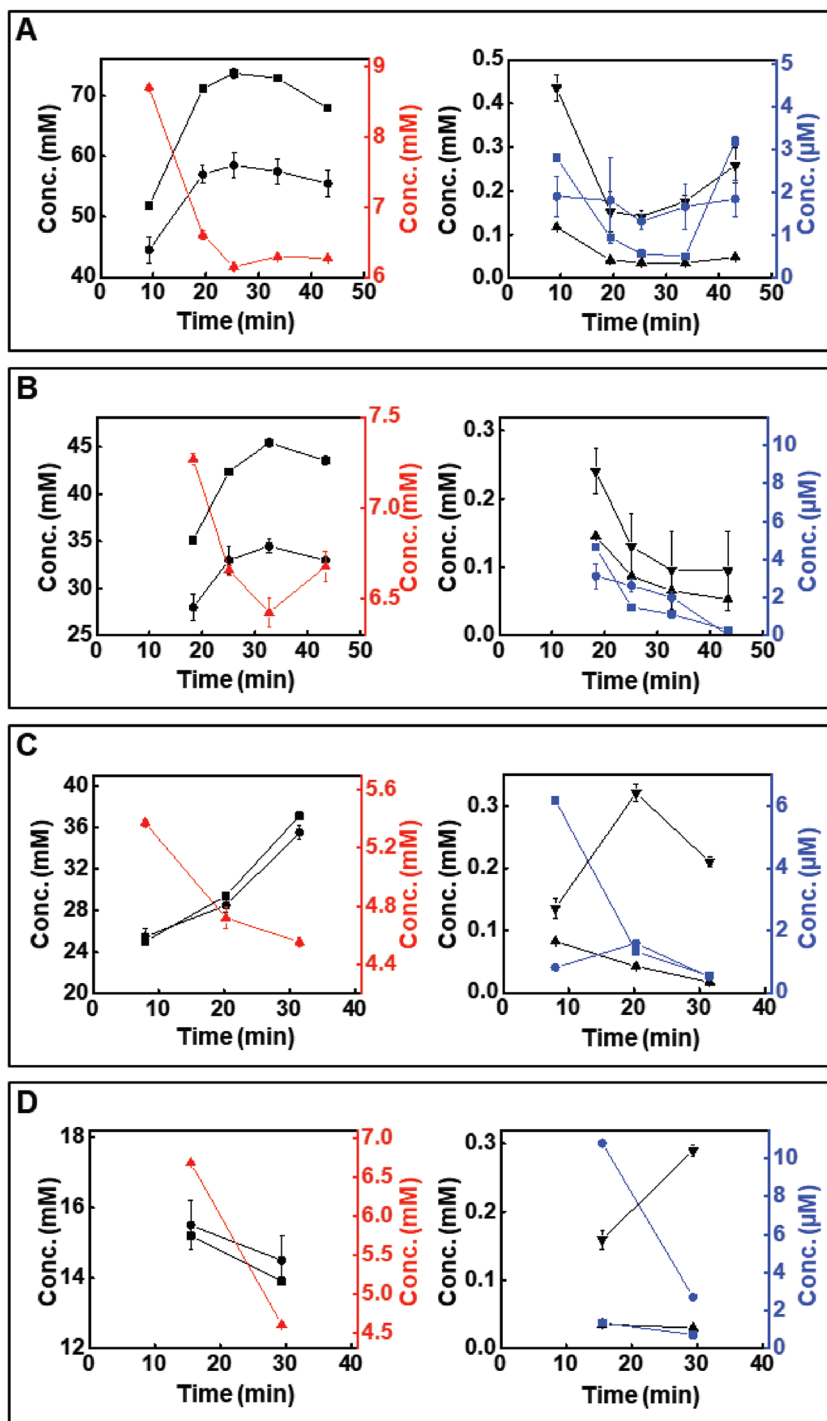


Figure 6. Time-dependent concentrations of sodium (■), chloride (●), potassium (▲), magnesium (▼), calcium (◆), copper (■), and iron (●) in sweat as measured by ICP-MS for devices filled to five (A), four (B), three (C), and two (D) chambers.

A second set of studies utilizes an ICP-MS system to measure temporal variations in the sodium, potassium, magnesium, calcium, iron, and copper and a chloridimeter to quantify chloride in sweat as a function of cycling intensity. Details appear in the Experimental Section (Supporting Information). **Figure 6** and **Figure S7** (Supporting Information)

show the data from these experiments. The tests reveal interesting trends in concentrations and their relation to time and sweat rate. Sweat sodium and chloride levels initially increase with time and then gradually decrease. Furthermore, in all studies the concentration of sodium is consistently higher than that of chloride. These observations are similar to previous studies and the data from the in situ colorimetric chloride sensor shown in **Figure 5** and **Figure S6** (Supporting Information).^[23,24] The plots indicate lower sweat rates as the subject becomes fatigued, which aligns with previously reported trends of these electrolytes with sweat rates.^[23–26] In contrast to the case of sodium and chloride, sweat potassium concentrations for high sweat rates begin at higher values before stabilizing to lower levels. The range of these stable concentration levels are similar to those recorded for low and medium sweat rate workouts. The decrease in potassium concentration to a stable value as a sweating session progresses is consistent with previous reports.^[24,27] The intensity of the cycling bout, and thus sweat rate, appears to have minimal impact on magnesium concentration. However, during a given workout bout the concentration gradually decreases with time, as observed in previous report.^[27] Calcium, on the other hand, demonstrates a temporal concentration profile that depends on sweat rate. At high sweat rates, the calcium concentration initially decreases and then gradually increases. At medium to low sweat rates, the concentration first increases and then decreases. The copper concentration shows an inverse relation with time, with slightly higher initial values for bouts involving higher sweat rates followed by rapid decrease and stabilization. Such a decrease in copper concentration with continued sweating is consistent with previous observations.^[27] The concentration of iron shows no clear trends. This set of experiments represents, to our knowledge, one of the broadest studies of temporal variations of sweat electrolytes and minerals during intraworkout bouts, but significant additional work is needed to establish significance in the observed trends.

Previous reports describe general trends in concentrations by measuring and comparing sweat samples collected during different workout sessions.^[24–27] Conventional sweat collection patches do not, however, allow intraworkout sweat analysis. Although recent examples of wearable sweat sensors are capable of real-time sweat biochemical analysis, present limitations in sensor technology address only a handful of analytes.^[2–4,28–30] The platform

described here permits temporal sweat analysis with any available analytical tool. These capabilities may allow for enhanced understanding of trends in minerals and electrolytes excreted in perspiration and their relation to workout duration and intensity. Sound understanding of these correlations will provide valuable information to nutritionists for personalizing dietary plans, to athletes for developing workout schedules, and to military personnel and workers who undergo high physical exertion during their daily routine. Similar studies utilizing this platform for analyzing other sweat biochemicals will further extend our understanding of the relation between physical activity and perspiration.

The results reported here demonstrate a unique approach to achieving comprehensive time-dynamic analysis of sweat biochemistry. The collection of materials, device architectures, and integration schemes involve an unusual combination of soft microfluidics, galvanic cell stopwatches, in situ colorimetrics, and ex situ analytical tools. Engineered soft microfluidic systems comprising of a series of chambers interconnected with passive valves enable chronometric collection of sweat samples with negligible intermixing, while galvanic cells offer a unique, battery-free approach to tracking the dynamics of sweat filling into the device. Detailed in vitro characterization of reproducibility, as well as the effects of mechanical stresses, ambient temperature variations, changes in flow rates, sweat composition, ionic strength, and inertial forces, serve as key studies in corroborating the robustness of the system. Human trials simulate real-life applications in which time-stamped sweat samples and ex situ chemical analysis determine temporal fluctuations in concentrations of sweat sodium, chloride, potassium, calcium, magnesium, copper, and iron throughout the course of an exercise routine. Compatibility with nearly any state-of-the-art analytical instrument, for a wide range of chemical assays, provides interesting capabilities in time-dependent sweat sampling. The results may create new opportunities for the study of correlations among sweat dynamics, chemistry, and physiology.

Supporting Information

Supporting Information is available from the Wiley Online Library or from the author.

Acknowledgements

A.J.B., J.C., and S.P.L. contributed equally to this work. This research was funded by the Air Force Research Laboratory (AFRL) Human Signatures Branch through Core funds provided to Northwestern University under contract FA8650-14-D-6516. This work utilized Northwestern University Micro/Nano Fabrication Facility (NUFAB), which is partially supported by Soft and Hybrid Nanotechnology Experimental (SHyNE) Resource (NSF ECCS-1542205), the Materials Research Science and Engineering Center (DMR-1720139), the State of Illinois, and Northwestern University. Metal analysis was performed at the Northwestern University Quantitative Bio-element Imaging Center generously supported by NASA Ames Research Center (Grant No.: NNA04CC36G). S.M. acknowledges support from Indo-U.S. Science and Technology Forum (Grant No.: SERB-IUSSTF-2017/192).

Conflict of Interest

J.A.R. and S.P.L. are cofounders of Epicore Biosystems, Inc., a company which pursues commercialization of microfluidic devices for wearable applications.

Keywords

colorimetry, galvanic cells, microfluidics, sweat sensing, wireless electronics

Received: April 2, 2019

Revised: May 5, 2019

Published online: June 17, 2019

- [1] C. J. Harvey, R. F. LeBouf, A. B. Stefaniak, *Toxicol. In Vitro* **2010**, *24*, 1790.
- [2] T. R. Ray, J. Choi, A. J. Bandodkar, S. Krishnan, P. Gutruf, L. Tian, R. Ghaffari, J. A. Rogers, *Chem. Rev.* **2019**, *119*, 5461.
- [3] J. Kim, A. S. Campbell, B. E.-F. de Ávila, J. Wang, *Nat. Biotechnol.* **2019**, *37*, 389.
- [4] M. Bariya, H. Y. Y. Nyein, A. Javey, *Nat. Electron.* **2018**, *1*, 160.
- [5] M. Delgado-Povedano, M. Calderón-Santiago, M. L. de Castro, F. Priego-Capote, *Talanta* **2018**, *177*, 47.
- [6] P. Kintz, A. Tracqui, P. Mangin, Y. Edel, *J. Anal. Toxicol.* **1996**, *20*, 393.
- [7] A. Koh, D. Kang, Y. Xue, S. Lee, R. M. Pielak, J. Kim, T. Hwang, S. Min, A. Banks, P. Bastien, M. C. Manco, L. Wang, K. R. Ammann, K.-I. Jang, P. Won, S. Han, R. Ghaffari, U. Paik, M. J. Slepian, G. Balooch, Y. Huang, J. A. Rogers, *Sci. Transl. Med.* **2016**, *8*, 366ra165.
- [8] J. Choi, D. Kang, S. Han, S. B. Kim, J. A. Rogers, *Adv. Healthcare Mater.* **2017**, *6*, 1601355.
- [9] J. Choi, A. J. Bandodkar, J. T. Reeder, T. R. Ray, A. Turnquist, S. B. Kim, N. Nyberg, A. I. Hourlier-Fargette, J. B. Model, A. J. Aranyosi, A. J. Aranyosi, S. Xu, R. Ghaffari, J. A. Rogers, *ACS Sens.* **2019**, *4*, 379.
- [10] A. J. Bandodkar, P. Gutruf, J. Choi, K. Lee, Y. Sekine, J. T. Reeder, W. J. Jeang, A. J. Aranyosi, S. P. Lee, J. B. Model, R. Ghaffari, C.-J. Su, J. P. Leshock, T. Ray, A. Verrillo, K. Thomas, V. Krishnamurthi, S. Han, J. Kim, S. Krishnan, T. Hang, J. A. Rogers, *Sci. Adv.* **2019**, *5*, eaav3294.
- [11] A. J. Bandodkar, *J. Electrochem. Soc.* **2017**, *164*, H3007.
- [12] W. Jia, G. Valdés-Ramírez, A. J. Bandodkar, J. R. Windmiller, J. Wang, *Angew. Chem., Int. Ed.* **2013**, *52*, 7233.
- [13] J. Choi, R. Ghaffari, L. B. Baker, J. A. Rogers, *Sci. Adv.* **2018**, *4*, eaar3921.
- [14] S. B. Kim, K. Lee, M. S. Raj, B. Lee, J. T. Reeder, J. Koo, A. Hourlier-Fargette, A. J. Bandodkar, S. M. Won, Y. Sekine, J. Choi, Y. Zhang, J. Yoon, B. H. Kim, Y. Yun, S. Lee, J. Shin, J. Kim, R. Ghaffari, J. A. Rogers, *Small* **2018**, *14*, 1802876.
- [15] J. Choi, Y. Xue, W. Xia, T. R. Ray, J. T. Reeder, A. J. Bandodkar, D. Kang, S. Xu, Y. Huang, J. A. Rogers, *Lab Chip* **2017**, *17*, 2572.
- [16] J. T. Reeder, J. Choi, Y. Xue, P. Gutruf, J. Hanson, M. Liu, T. Ray, A. J. Bandodkar, R. Avila, W. Xia, S. Krishnan, S. Xu, K. Barnes, M. Pahnke, R. Ghaffari, Y. Huang, J. A. Rogers, *Sci. Adv.* **2019**, *5*, eaau6356.
- [17] V. K. Samineneni, J. Yoon, K. E. Crawford, Y. R. Jeong, K. C. McKenzie, G. Shin, Z. Xie, S. S. Sundaram, Y. Li, M. Y. Yang, J. Kim, D. Wu, Y. Xue, X. Feng, Y. Huang, A. D. Mickle, A. Banks, J. S. Ha, J. P. Golden, J. A. Rogers, R. W. Gereau, *PAIN* **2017**, *158*, 2108.

- [18] Y.-M. Tang, D.-G. Wang, J. Li, X.-H. Li, Q. Wang, N. Liu, W.-T. Liu, Y.-X. Li, *Ind. Health* **54**, **2016**, 215.
- [19] C. F. Consolazio, L. O. Matoush, R. A. Nelson, R. S. Harding, J. E. Canham, *J. Nutr.* **1963**, *79*, 407.
- [20] H. C. Lukaski, *Int. J. Sport Nutr.* **1995**, *5*, S74.
- [21] N. Kondo, S. Takano, K. Aoki, M. Shibasaki, H. Tominaga, Y. Inoue, *Acta Physiol. Scand.* **1998**, *164*, 71.
- [22] A. J. Bandodkar, W. J. Jeang, R. Ghaffari, J. A. Rogers, *Annu. Rev. Anal. Chem.* **2019**, *12*, 061318.
- [23] M. J. Buono, K. D. Ball, F. W. Kolkhorst, *J. Appl. Physiol.* **2007**, *103*, 990.
- [24] H. M. Emrich, E. Stoll, B. Friolet, J. P. Colombo, R. Richterich, E. Rossi, *Pediatr. Res.* **1968**, *2*, 464.
- [25] G. W. Cage, R. L. Dobson, *J. Clin. Invest.* **1965**, *44*, 1270.
- [26] D. B. Dill, F. G. Hall, W. V. Beaumont, *J. Appl. Physiol.* **1966**, *21*, 99.
- [27] S. J. Montain, S. N. Chevront, H. C. Lukaski, *Int. J. Sport Nutr. Exercise Metab.* **2007**, *17*, 574.
- [28] W. Gao, H. Y. Nyein, Z. Shahpar, H. M. Fahad, K. Chen, S. Emaminejad, Y. Gao, L.-C. Tai, H. Ota, E. Wu, J. Bullock, Y. Zeng, D.-H. Lien, A. Javey, *ACS Sens.* **2016**, *1*, 866.
- [29] J. Kim, W. R. de Araujo, I. A. Samek, A. J. Bandodkar, W. Jia, B. Brunetti, T. R. Paixão, J. Wang, *Electrochem. Commun.* **2015**, *51*, 41.
- [30] Y. Sekine, S. B. Kim, Y. Zhang, A. J. Bandodkar, S. Xu, J. Choi, M. Irie, T. R. Ray, P. Kohli, N. Kozai, T. Sugita, Y. Wu, K. Lee, K.-T. Lee, R. Ghaffari, J. A. Rogers, *Lab Chip* **2018**, *18*, 2178.